Rossby Wave Propagation and Teleconnection Patterns in the Austral Winter

Ambrizzi, T., B.J. Hoskins, and H. Hsu, 1995: Rossby Wave Propagation and Teleconnection Patterns in the Austral Winter. J. Atmos. Sci., 52, 3661–3672

Bruna Ferreira Ramim
2019

Divisão do artigo

1. Introdução
2. Teleconectividade
3. Evolução temporal
    a. Hemisfério Sul
    b. Hemisfério Norte
    c. Sumário
4. Estado básico, teoria, e o modelo barotrópico
5. Resultados do modelo barotrópico
    a. Jatos subtropical e polar
    b. Atlântico Sul
    c. Pacífico leste e sudeste
    d. Jato do Atlântico Norte
    e. Jato norte africano-asiático
6. Conclusões
7. Referências

1. Introdução

- Análise das teleconexões: visão global das anomalias locais na circulação atmosférica e suas influências na circulação de regiões remotas

- Mais estudos focados no Hemisfério Norte (HN) do que no Hemisfério Sul (HS)

- Frequências:
  - Alta frequência (ondas baroclínicas)
  - Intermediária: período de 10 a 30 dias (estrutura ondulatória - dispersão de energia por trens de onda estacionários)
  - Baixa: período maior que 30 dias

- Objetivo: apresentar evidências observacionais e numéricas dos padrões de teleconexões no HN e HS que exibem comportamentos característicos de ondas de Rossby em Junho-Julho-Agosto (JJA) => inverno austral

2. Teleconectividade

- Dados: ECMWF (European Centre for Medium-Range Weather Forecasts)
  - Inicializados 12 UTC
  - Média para 11 períodos de Junho a Agosto (1979 -1989)
  - Vento em 200 hPa (grade 5º x 5º)

- Função de corrente a partir da vorticidade

- Subtração das médias zonais
  - Padrão zonalmente simétrico identificado nos invernos do HN por Hsu e Lin em 1992
  - Há nos invernos austrais esse mesmo padrão, que tende a mascarar a estrutura ondulatória dos padrões de teleconexões

- Filtro: 10 - 30 dias

- Estrutura de teleconexão mascarada na mapa de função de corrente ⇔ mapa de teleconectividade (Wallace e Gutzler, 1981)

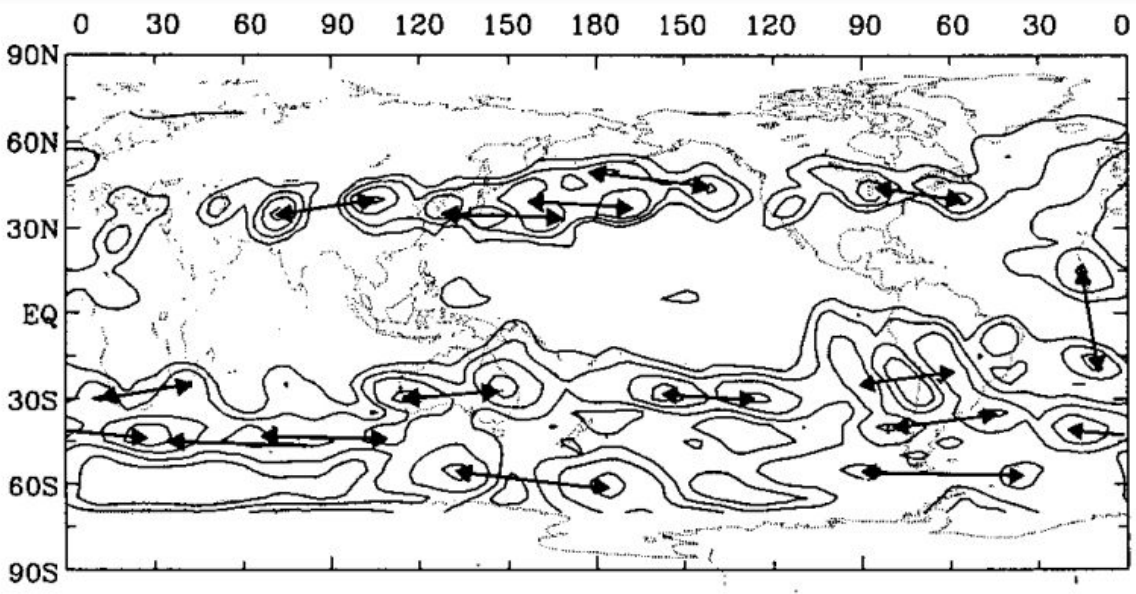

FIG. 1. Teleconnectivity of 10–30-day bandpass-filtered eddy streamfunction at 200 hPa. The values have been multiplied by 100; values smaller than 40 are not contoured, and the contour interval is 5. Locations of maximum teleconnectivity are indicated by the arrows.

=> 2088 mapas de correlações pontuais para pontos base a cada 5º de latitude e longitude (entre 70ºN e 70ºS)
=> Setas indicam máximos de teleconectividade

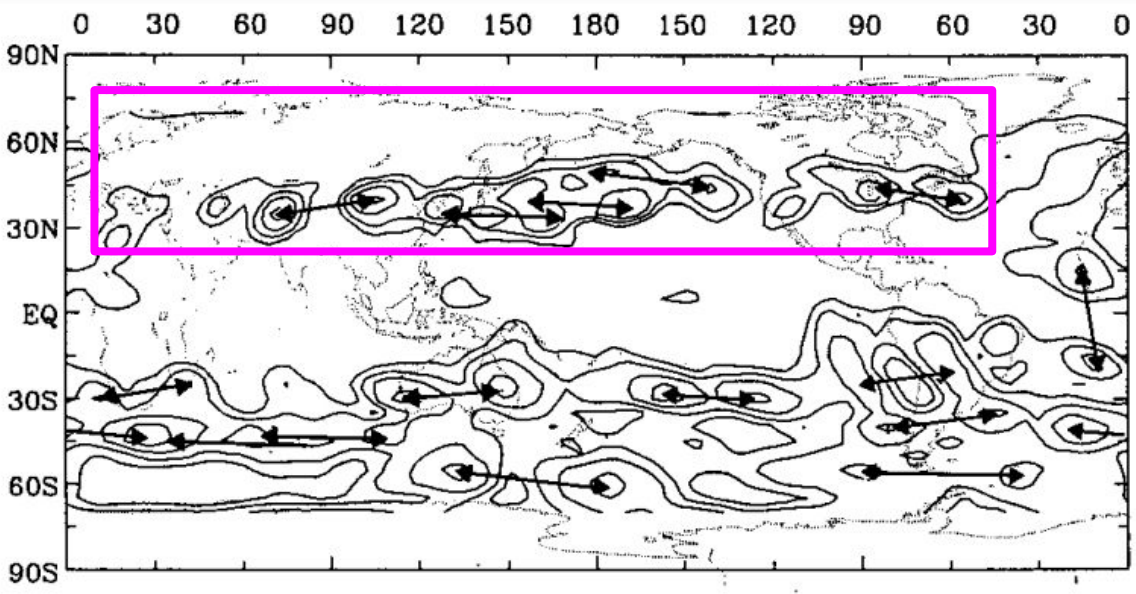

FIG. 1. Teleconnectivity of 10–30-day bandpass-filtered eddy streamfunction at 200 hPa. The values have been multiplied by 100; values smaller than 40 are not contoured, and the contour interval is 5. Locations of maximum teleconnectivity are indicated by the arrows.

=> Assim como encontrado para DJF, no HN as regiões de mais forte teleconexões estão perto do jato asiático e atlântico, orientadas quase que zonalmente

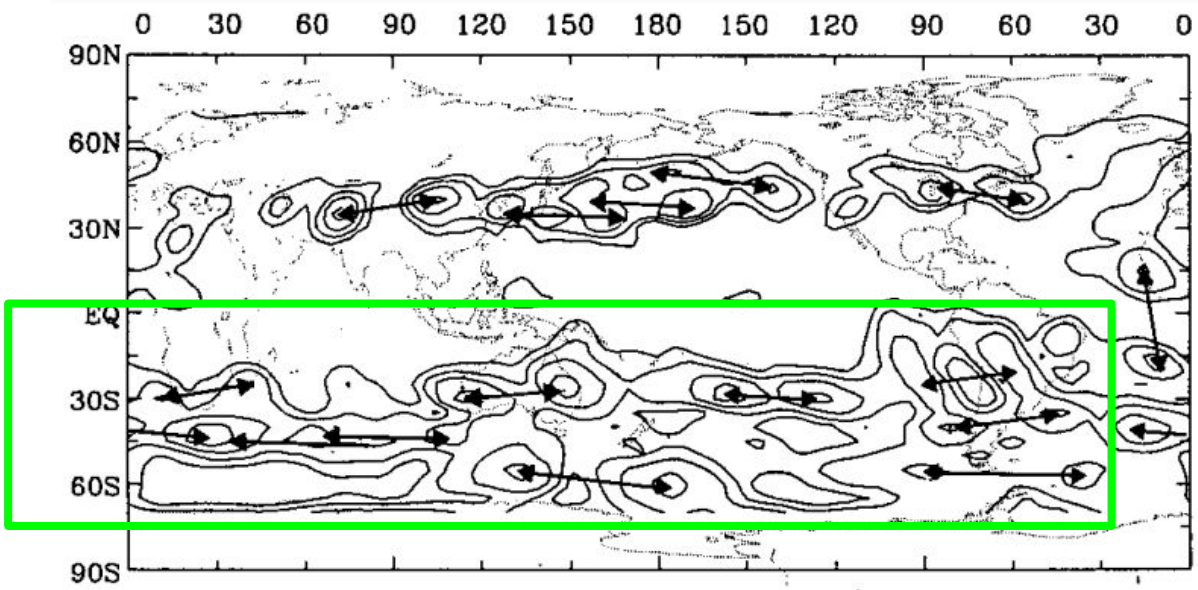

FIG. 1. Teleconnectivity of 10–30-day bandpass-filtered eddy streamfunction at 200 hPa. The values have been multiplied by 100; values smaller than 40 are not contoured, and the contour interval is 5. Locations of maximum teleconnectivity are indicated by the arrows.

=> Em JJA a localização dos máximos de correlação está mais norte do que em DJF e os valores são menores
=> 6 regiões de destaque: 1) Austrália; 2) Pacífico Sul subtropical; 3) América do Sul; 4) Oceano Índico e Atlântico subtropicais e regiões polares perto de 60°S; 5) entre 120°E e 180° e 6) entre 80°W e 30°W

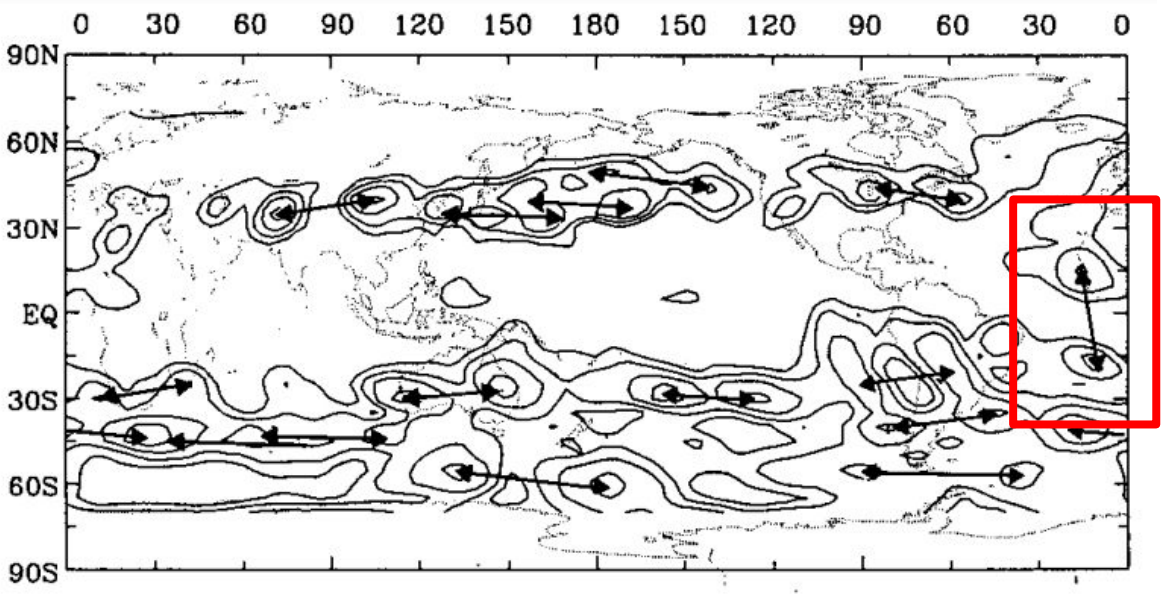

FIG. 1. Teleconnectivity of 10–30-day bandpass-filtered eddy streamfunction at 200 hPa. The values have been multiplied by 100; values smaller than 40 are not contoured, and the contour interval is 5. Locations of maximum teleconnectivity are indicated by the arrows.

=> Assim como no HN, no HS as regiões de forte teleconectividade tendem a estar zonalmente orientadas e coincidem com a localização das correntes de jato

=> No Atlântico tropical há uma região orientada meridionalmente

3. Evolução Temporal

- Investigação da estrutura e evolução temporal dos padrões de teleconexões através das correlações cruzadas e defasadas no tempo entre os pontos de maior teleconectividade identificados na figura 1 e os outros pontos de grade

- 8 pontos base serão mostrados

- Os graus de liberdade para os mapas de correlação mostrados foram calculados assim como em Hsu e Lin (1992) e indicam que os graus de liberdade são >>100

- Assumindo 60 graus de liberdade:
  - Correlações acima de 0.3 para rejeitar a hipótese nula de não correlação ao nível de significância de 0.01
  - Correlações acima de 0.25 para rejeitar a hipótese nula de não correlação ao nível de significância de 0.025
  - Nos próximos mapas são plotados apenas pontos com valores absolutos maiores que 0.2

a) Hemisfério Sul

- Ponto base: 30ºS,120ºW
- Dia -3: estrutura de onda a oeste do ponto base ao longo de 30ºS (escala zonal ~nº de onda 6)
- Dia 0: desenvolvimento de novas células a nordeste do ponto base, e as células a oeste se enfraquecem; o fluxo para ser direcionado ao Equador
- Dia +3: outra estrutura ondulatória cruza o sul do continente sul americano e a parte que parecia ir para o Equador enfraquece
- Durante o desenvolvimento de novas células ao longo do escoamento, os centros individuais de máxima correlação se movem para leste (~20º de latitude em 6 dias => 3m/s)

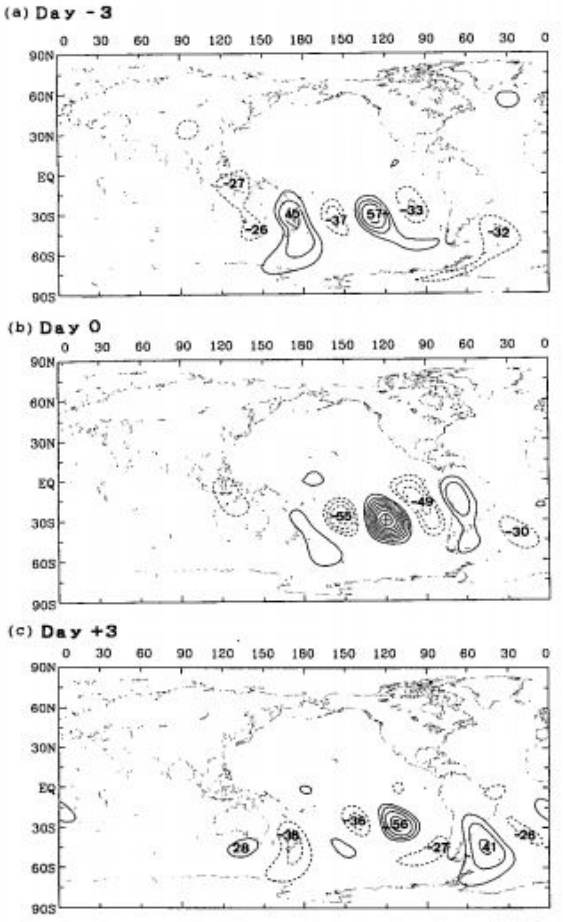

FIG. 2. Lag correlation between the streamfunction at (30°S, 120°W) and streamfunction at every point (a) 3 days earlier, (b) day 0, and (c) 3 days later. The values have been multiplied by 100; values between −20 and 20 are not contoured. Negative values are dashed, and the contour interval is 10. The location of the base point, (30°S, 120°W), is marked by a cross sign.

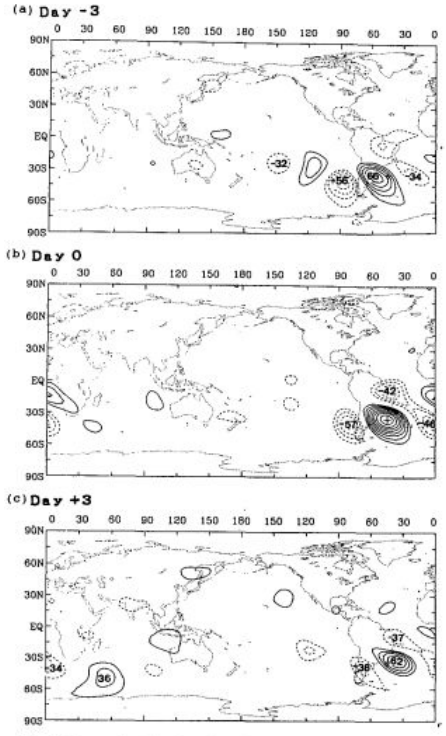

FIG. 3. Same as in Figs. 2a–c but for base point (35°S, 45°W).

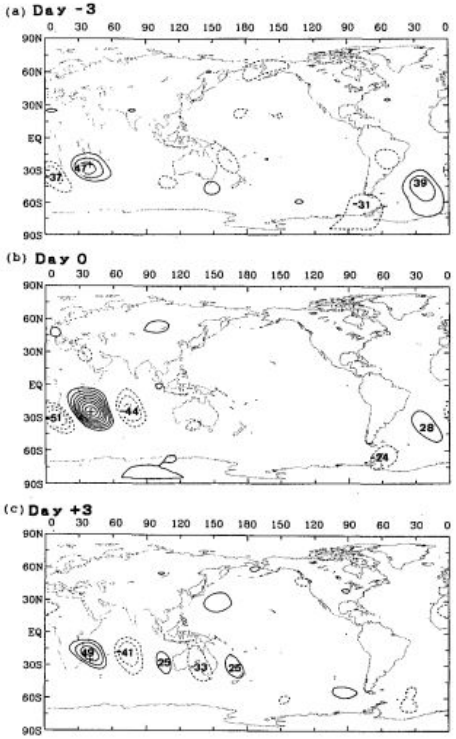

FIG. 4. Same as in Figs. 2a–c but for base point (25°S, 40°E).

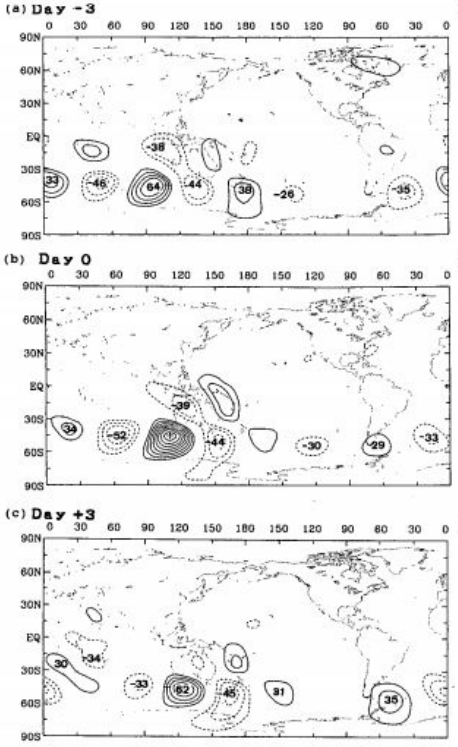

FIG. 5. Same as in Figs. 2a–c but for base point (45°S, 110°E).

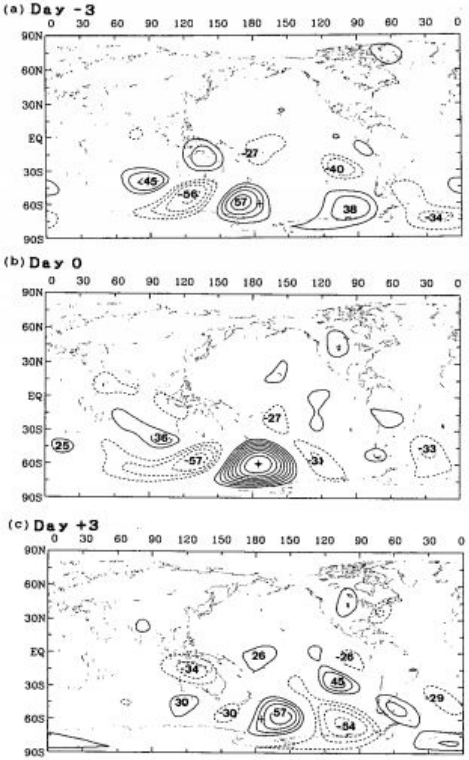

FIG. 6. Same as in Figs. 2a–c but for base point (60°S, 175°W).

b) Hemisfério Norte

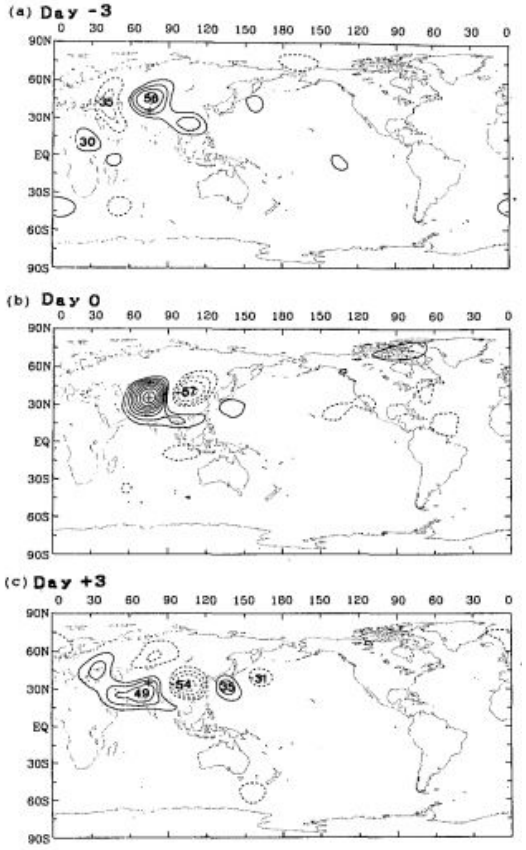

FIG. 7. Same as in Figs. 2a–c but for base point (35°N, 75°E).

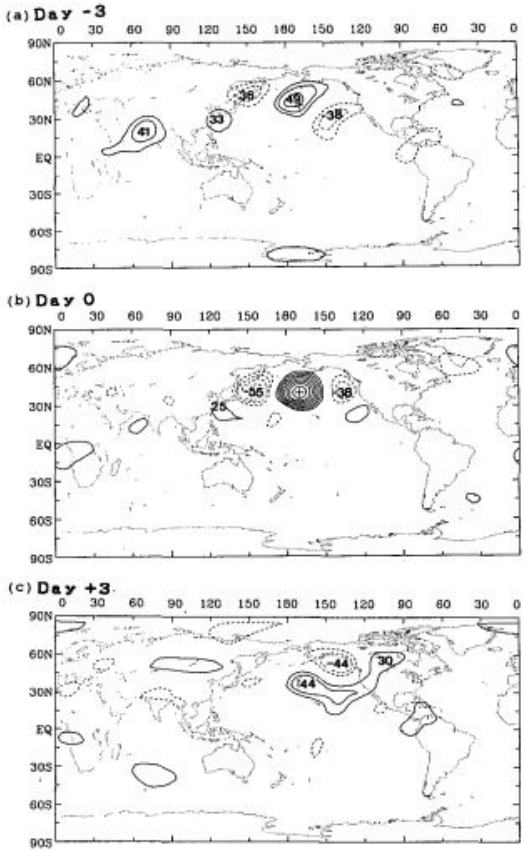

FIG. 8. Same as in Figs. 2a–c but for base point (40°N, 170°W).

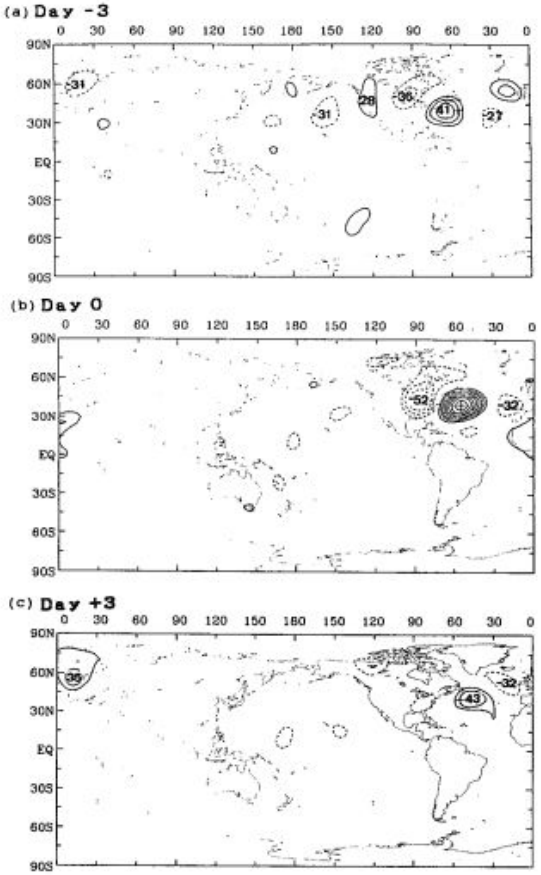

FIG. 9. Same as in Figs. 2a–c but for base point (40°N, 55°W).

c) Sumário

- Determinação de rotas na alta troposfera ao longo das quais os padrões de teleconexões parecem se desenvolver (baseando-se nos mapas de correlação)

- Correntes de jato => localização favorita para as rotas de propagação

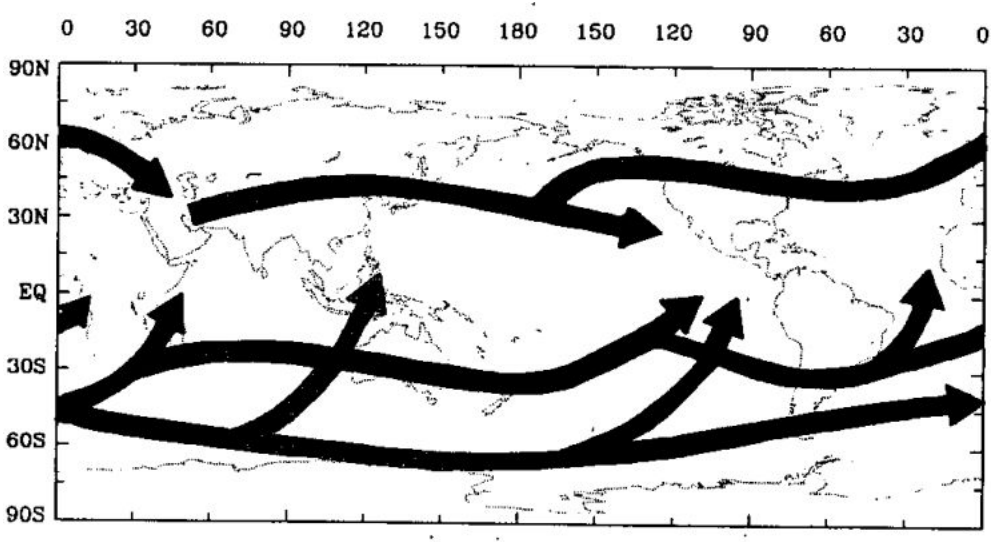

FIG. 10. Schematic plot of teleconnection propagation routes deduced from numerous lag correlation maps for the base points from 70°N to 70°S for every 10° of latitude and longitude.

- Cálculo das estatísticas das correlações com *lag* para pontos base a cada 10º de latitude e longitude, entre 20ºN e 20ºS

  => Investigar a força da propagação em direção ao Equador, que é mais encontrada no HS no oceano Índico, Pacífico oeste e América do Sul

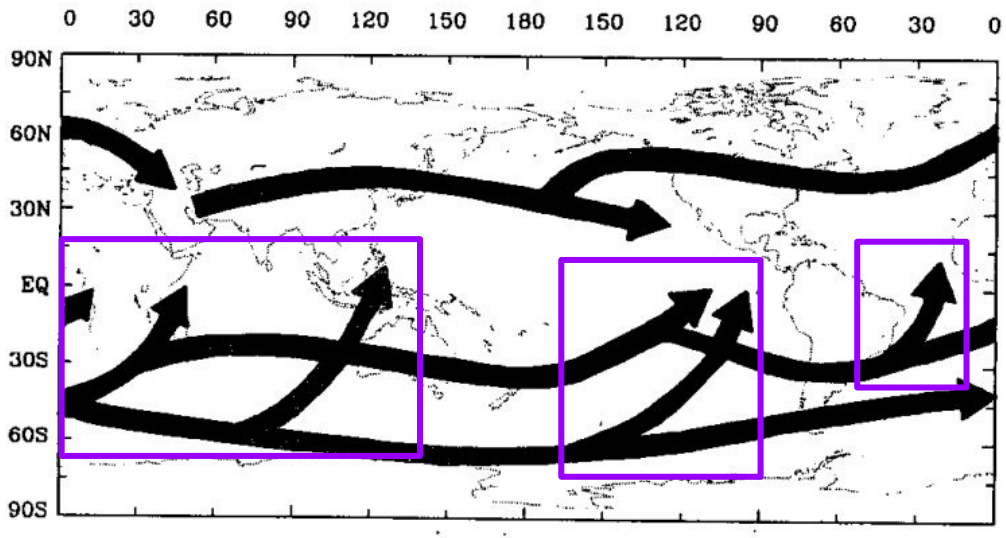

FIG. 10. Schematic plot of teleconnection propagation routes deduced from numerous lag correlation maps for the base points from 70°N to 70°S for every 10° of latitude and longitude.

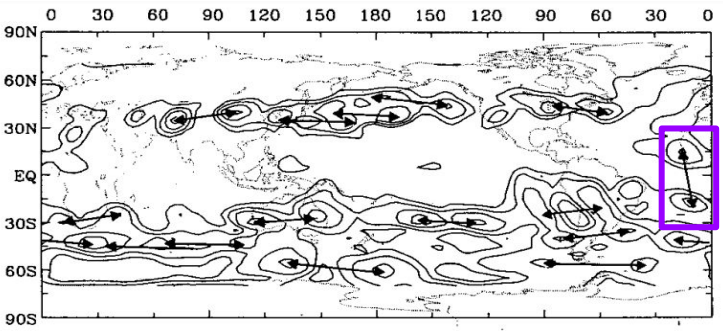

FIG. 1. Teleconnectivity of 10–30-day bandpass-filtered eddy streamfunction at 200 hPa. The values have been multiplied by 100; values smaller than 40 are not contoured, and the contour interval is 5. Locations of maximum teleconnectivity are indicated by the arrows.

=> Dipolo que que se move lentamente para oeste e não tem estrutura de onda; movimento para oeste é característica comum dos padrões de teleconexões entre 20ºN e 20ºS

=> Hsu e Lin (1992): propagação que cruza o Equador ocorre apenas em DJF na região dos ventos de oeste no Equador

=>JJA: prevalecem os ventos de leste na alta troposfera tropical

=> A interação extratrópicos-trópicos na alta troposfera é maior no hemisfério de inverno

=> A orientação de cada célula no padrão de teleconexão tende a ser perpendicular a rota ao longo da qual os sucessivos desenvolvimentos de novas células ocorrem

=> Interpretação: <u>Dispersão de ondas de Rossby</u>

4. Estado básico, teoria, e o modelo barotrópico

- Hoskins e Ambrizzi (1993): as observações e os resultados dos modelos para DJF podiam ser entendidos pela propagação de ondas de Rossby

- Número de onda estacionário de Rossby:

$$K_s = (\beta_* / \bar{U})^{1/2}$$

=> β_* é o gradiente de vorticidade absoluta
=> $\overline{U}$ é o vento de oeste

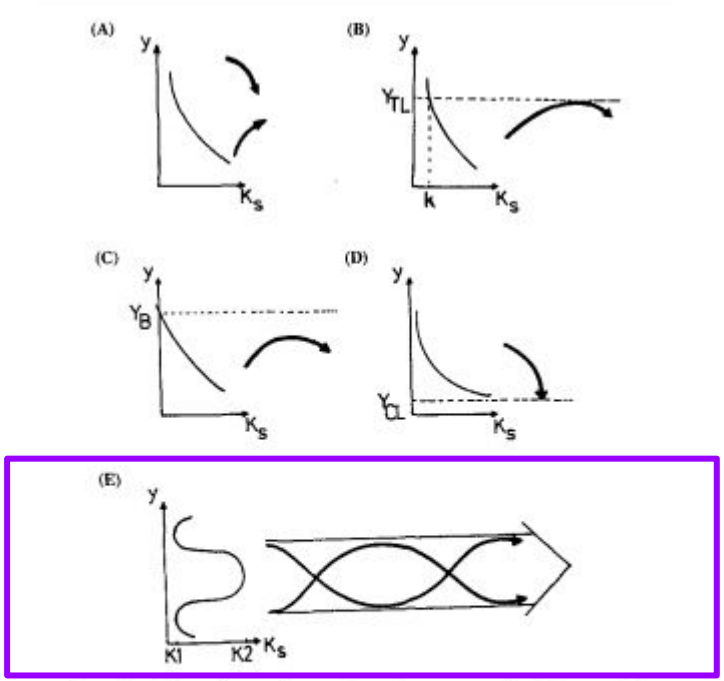

FIG. 2. Schematic stationary Rossby wavenumber (K_s) profiles and ray path refraction. In each panel, K_s is shown as a function of y and schematic ray paths are shown by heavy lines with arrowheads. (a) simple refraction; (b) reflection from a turning latitude Y_{TL} at which $K_s = k$; (c) reflection of all wavenumbers before a latitude Y_B at which $\beta_* = 0$; (d) refraction into a critical latitude Y_{CL} at which $\bar{U} = 0$; (e) waveguide effect of a K_s maximum. For more discussion see text.

=> Guia de onda
=> Situação ocorre nas correntes de jato de oeste
=> Jatos podem ser guias de ondas de Rossby

Figura 2 extraída de Hoskins, B.J. and T. Ambrizzi, 1993: Rossby Wave Propagation on a Realistic Longitudinally Varying Flow. J. Atmos. Sci., 50, 1661–1671

- Estado básico em 300 hPa (concordando com os estudos barotrópicos e baroclínicos)

- Média temporal de JJA de 6 anos (1979-1985) [ECMWF]

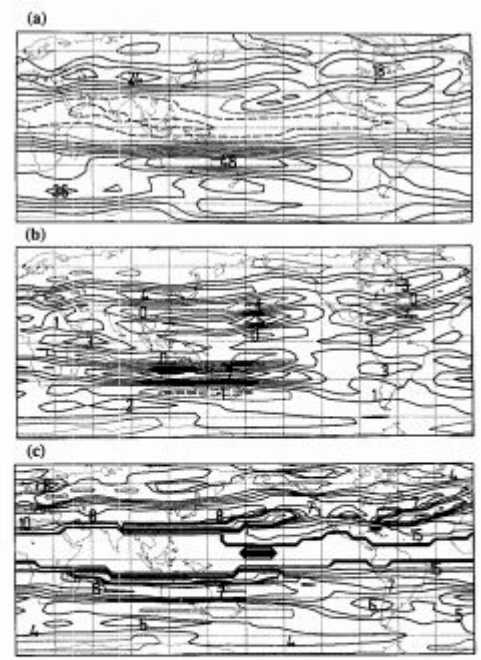

FIG. 11. The climatological JJA 300-hPa flow based on ECMWF data for the period 1979–85. (a) Westerly component of the wind U; contour interval is 6 m s^{-1}. (b) Mercator coordinate meridional gradient of the absolute vorticity β_m [defined by Eq. (2.12) in HA]; contour interval is 1×10^{-11} s^{-1} m^{-1}. (c) Stationary wavenumber K_s [defined by Eq. (2.13) in HA] for β_m and $\bar{U}$ positive; contours for wavenumbers 0, 4, 5, 6, 7, 8, 10, and 15, and also 25–30, producing a thickened contour indicating singular values of K_s. The position of this thickened contour differs slightly from that of the $\bar{U} = 0$ contour in (a) mainly because of differences obtained by interpolating very differently behaved quantities on a finite grid. In all panels, negative contours are dashed, and zero contours are dotted. Lines of latitude and longitude are drawn every 30°.

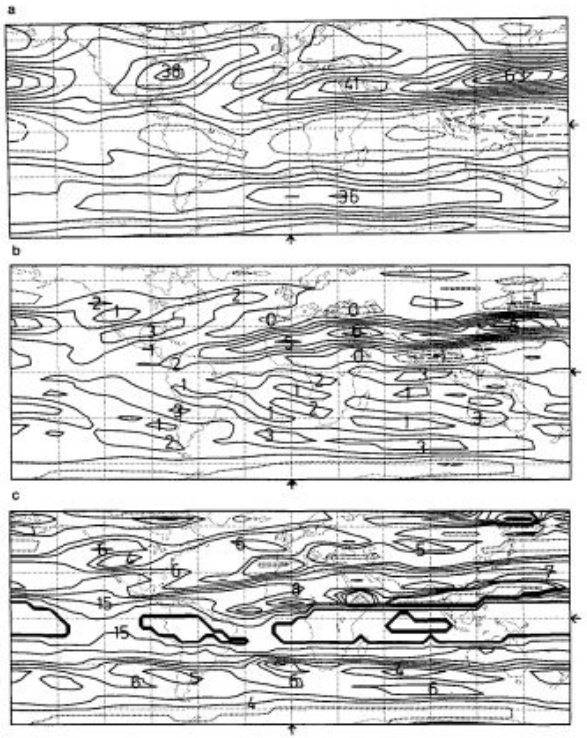

FIG. 3. The climatological DJF 300-mb flow based on ECMWF data for the period 1979–85. (a) Westerly component of the wind, U; contour interval 6 m s^{-1}. (b) Mercator coordinate meridional gradient of the absolute vorticity, β_M, defined in (2.12); contour interval 1.10^{-11} s^{-1} m^{-1}. (c) Stationary wavenumber, K_s, defined in (2.13) for β_M and $\bar{U}$ positive; contours at zonal wavenumbers 0, 4, 5, 6, 7, 8, 10, and 15, and also 25–30, producing a thickened contour indicating singular values of K_s. In all panels, negative contours are dashed and zero contours are dotted. Lines of latitude and longitude are drawn every 30°, and arrows indicate 0° latitude and longitude.

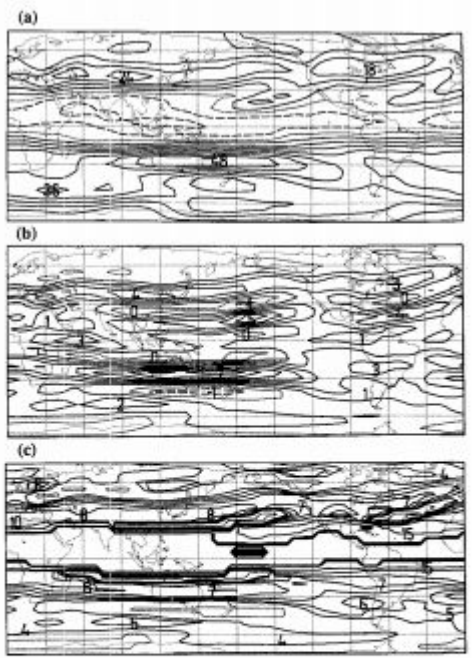

FIG. 11. The climatological JJA 300-hPa flow based on ECMWF data for the period 1979–85. (a) Westerly component of the wind U; contour interval is 6 m s^{-1}. (b) Mercator coordinate meridional gradient of the absolute vorticity β_M [defined by Eq. (2.12) in HA]; contour interval is 1×10^{-11} s^{-1} m^{-1}. (c) Stationary wavenumber K_s [defined by Eq. (2.13) in HA] for β_M and $\bar{U}$ positive; contours for wavenumbers 0, 4, 5, 6, 7, 8, 10, and 15, and also 25–30, producing a thickened contour indicating singular values of K_s. The position of this thickened contour differs slightly from that of the $\bar{U} = 0$ contour in (a) mainly because of differences obtained by interpolating very differently behaved quantities on a finite grid. In all panels, negative contours are dashed, and zero contours are dotted. Lines of latitude and longitude are drawn every 30°.

Figura 3 extraída de Hoskins, B.J. and T. Ambrizzi, 1993: Rossby Wave Propagation on a Realistic Longitudinally Varying Flow. J. Atmos. Sci., 50, 1661–1671

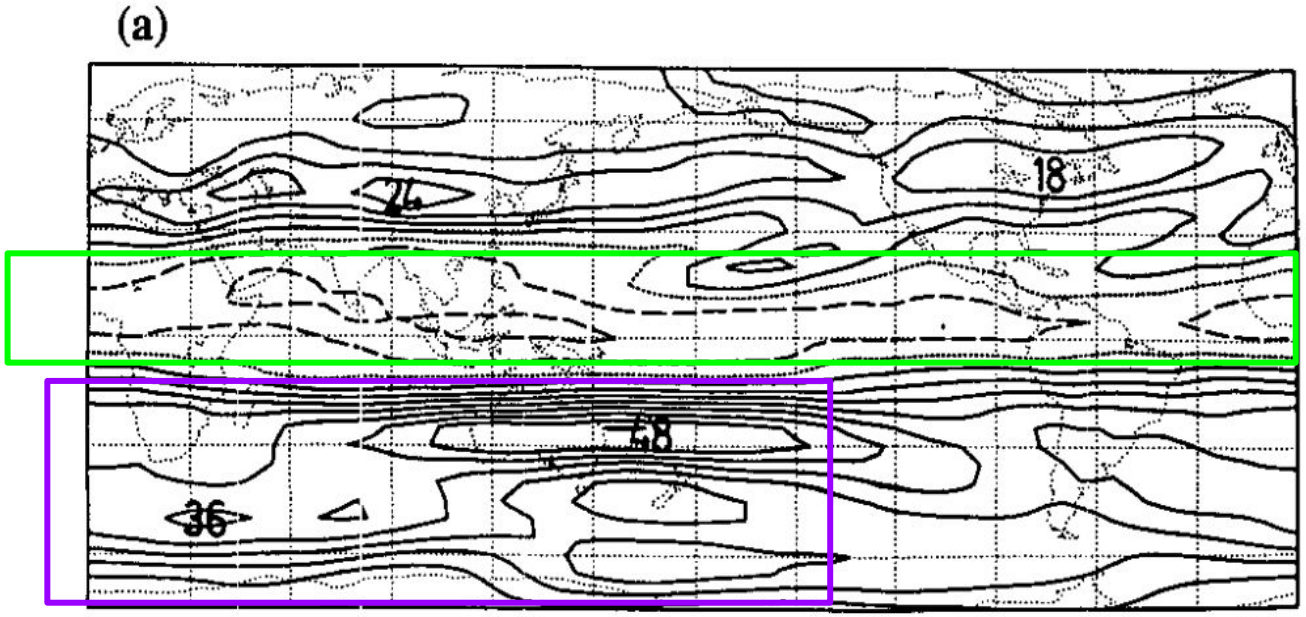

Vento de leste na região tropical ⇔ não favorece propagações que cruzam o Equador

Inverno HS: dois jatos

FIG. 11. The climatological JJA 300-hPa flow based on ECMWF data for the period 1979–85. (a) Westerly component of the wind U; contour interval is 6 m s^{-1}. (b) Mercator coordinate meridional gradient of the absolute vorticity β_m [defined by Eq. (2.12) in HA]; contour interval is 1×10^{-11} s^{-1} m^{-1}. (c) Stationary wavenumber K_s [defined by Eq. (2.13) in HA] for β_m and $\bar{U}$ positive; contours for wavenumbers 0, 4, 5, 6, 7, 8, 10, and 15, and also 25–30, producing a thickened contour indicating singular values of K_s. The position of this thickened contour differs slightly from that of the $\bar{U} = 0$ contour in (a) mainly because of differences obtained by interpolating very differently behaved quantities on a finite grid. In all panels, negative contours are dashed, and zero contours are dotted. Lines of latitude and longitude are drawn every 30°.

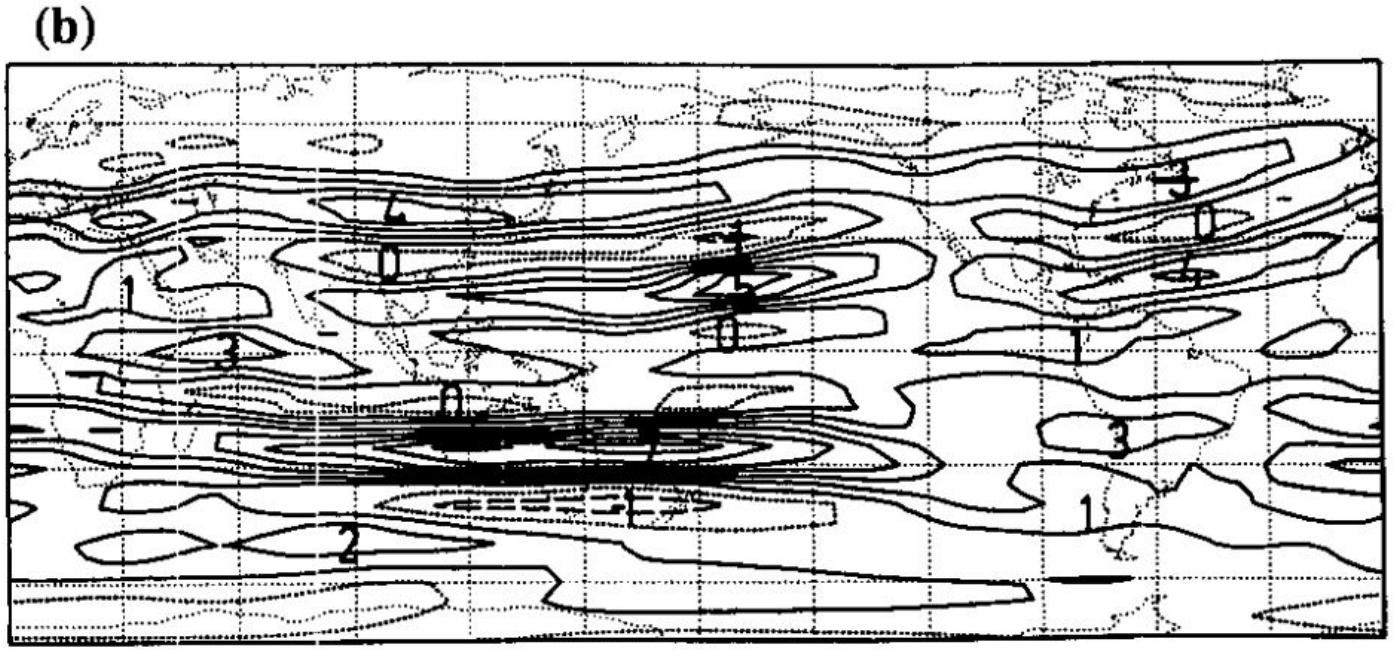

=> β_m máxima nos jatos e mínima no norte e sul

FIG. 11. The climatological JJA 300-hPa flow based on ECMWF data for the period 1979–85. (a) Westerly component of the wind U; contour interval is 6 m s^{-1}. (b) Mercator coordinate meridional gradient of the absolute vorticity β_m [defined by Eq. (2.12) in HA]; contour interval is 1×10^{-11} s^{-1} m^{-1}. (c) Stationary wavenumber K_s [defined by Eq. (2.13) in HA] for β_m and $\bar{U}$ positive; contours for wavenumbers 0, 4, 5, 6, 7, 8, 10, and 15, and also 25–30, producing a thickened contour indicating singular values of K_s. The position of this thickened contour differs slightly from that of the $\bar{U} = 0$ contour in (a) mainly because of differences obtained by interpolating very differently behaved quantities on a finite grid. In all panels, negative contours are dashed, and zero contours are dotted. Lines of latitude and longitude are drawn every 30°.

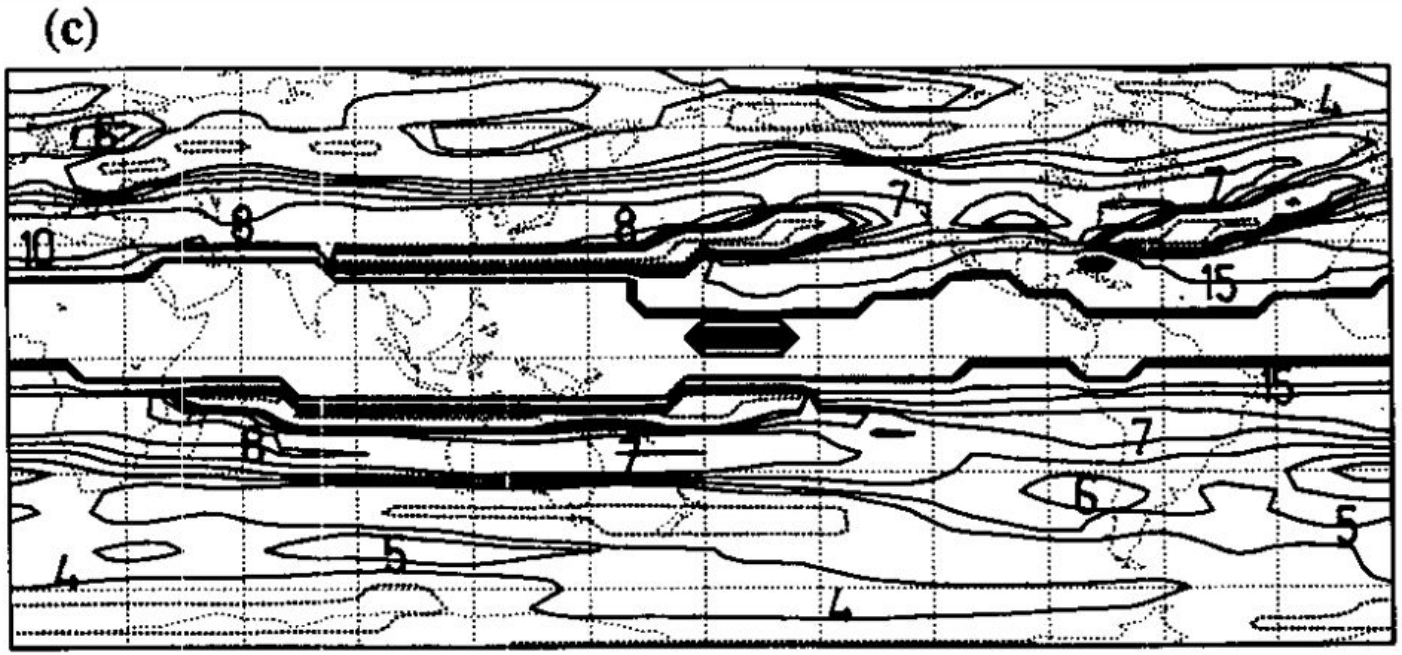

=> Jatos: valores uniformes de Ks cercados meridionalmente por valores menores ⇔ guia de ondas

=> Semelhança com a Figura 1

FIG. 11. The climatological JJA 300-hPa flow based on ECMWF data for the period 1979–85. (a) Westerly component of the wind U; contour interval is 6 m s^{-1}. (b) Mercator coordinate meridional gradient of the absolute vorticity β_m [defined by Eq. (2.12) in HA]; contour interval is 1×10^{-11} s^{-1} m^{-1}. (c) Stationary wavenumber K_s [defined by Eq. (2.13) in HA] for β_m and $\bar{U}$ positive; contours for wavenumbers 0, 4, 5, 6, 7, 8, 10, and 15, and also 25–30, producing a thickened contour indicating singular values of K_s. The position of this thickened contour differs slightly from that of the $\bar{U} = 0$ contour in (a) mainly because of differences obtained by interpolating very differently behaved quantities on a finite grid. In all panels, negative contours are dashed, and zero contours are dotted. Lines of latitude and longitude are drawn every 30°.

5. Resultados do modelo barotrópico

- Equação da vorticidade barotrópica não divergente
- Forçantes

a) Jato subtropical e polar

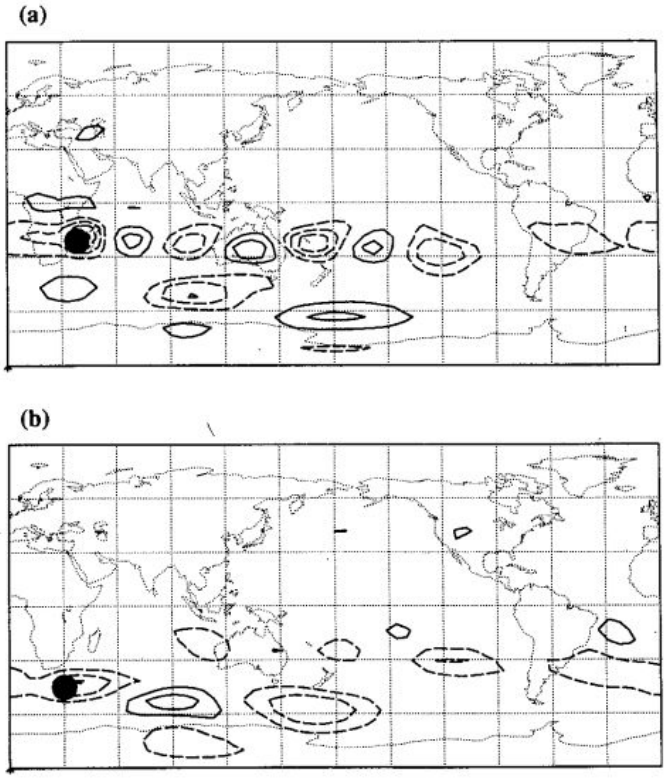

FIG. 12. The model vorticity anomaly for the forcing centered at (a) (20°S, 40°E) and (b) (45°S, 30°E) at day 12. The contour interval is 5×10^{-6} s^{-1}; negative values are dashed, and the zero contour is not shown. The black circle indicates the forcing position.

- Aplicação das forçantes circulares na entrada dos jatos polares e subtropicais

- Há propagação de ondas de Rossby ao longo da corrente de jato australiana

- Figura 4c

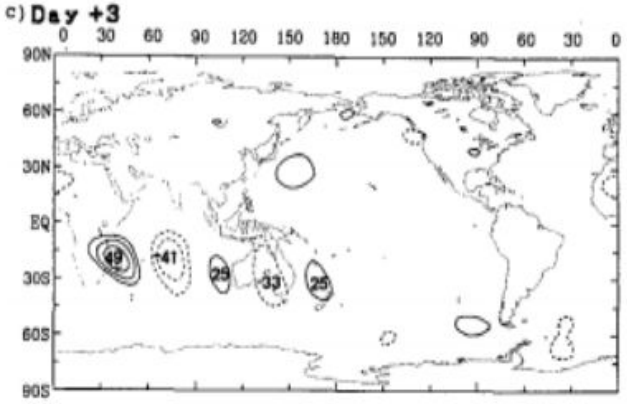

FIG. 4. Same as in Figs. 2a–c but for base point (25°S, 40°E).

b) Atlântico Sul

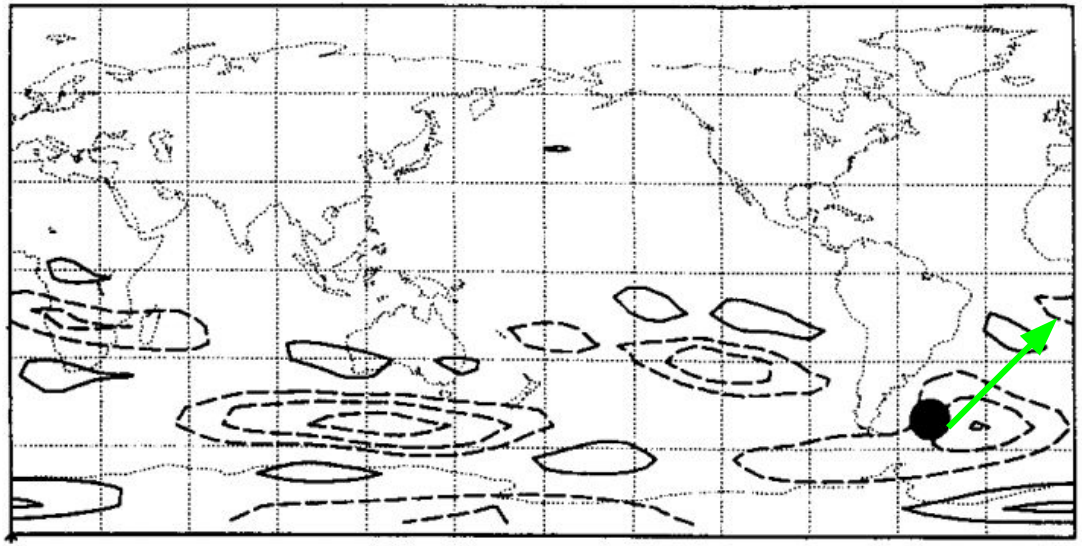

FIG. 13. The model vorticity anomaly at day 12 for the forcing at (50°S, 50°W). Contour conventions as in Fig. 12.

- 3 caminhos:

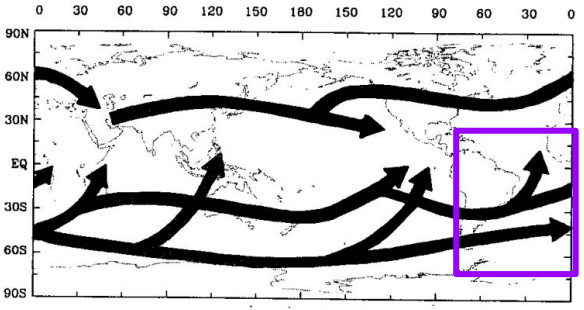

FIG. 10. Schematic plot of teleconnection propagation routes deduced from numerous lag correlation maps for the base points from 70°N to 70°S for every 10° of latitude and longitude.

c) Pacífico leste e sudeste

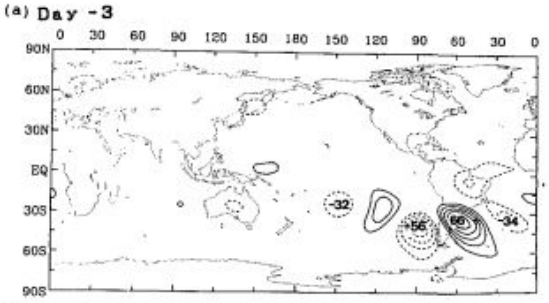

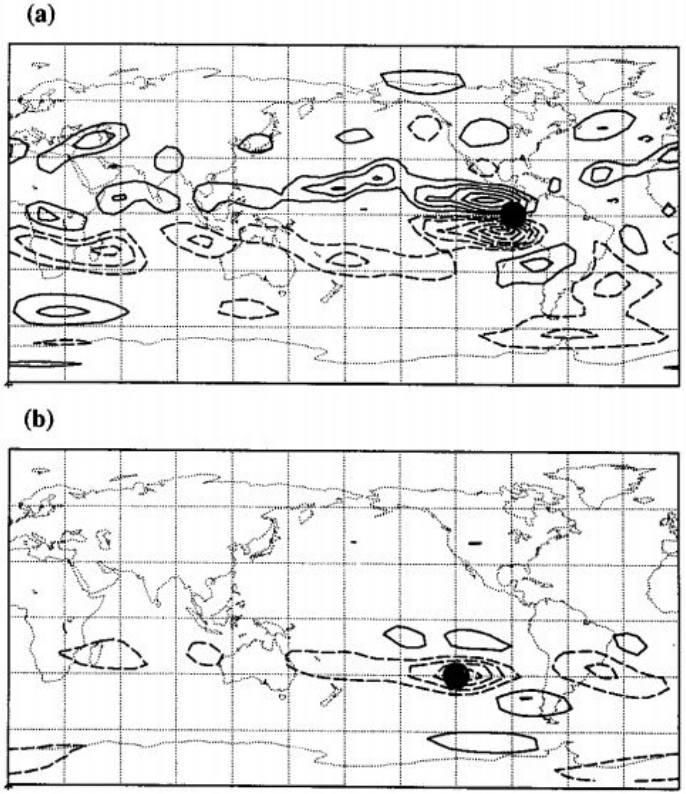

FIG. 14. The model vorticity anomaly for the forcing centered at (a) (0°, 90°W) and (b) (30°S, 120°W) at day 12. Contour conventions as in Fig. 12.

- Divisão da onda
- Fig 2a e 3a

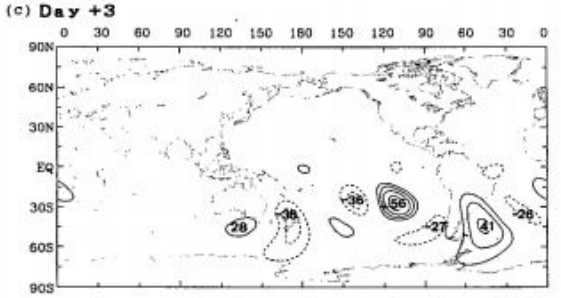

FIG. 2. Lag correlation between the streamfunction at (30°S, 120°W) and streamfunction at every point (a) 3 days earlier, (b) day 0, and (c) 3 days later. The values have been multiplied by 100; values between −20 and 20 are not contoured. Negative values are dashed, and the contour interval is 10. The location of the base point, (30°S, 120°W), is marked by a cross sign.

d) Jato do Atlântico Norte

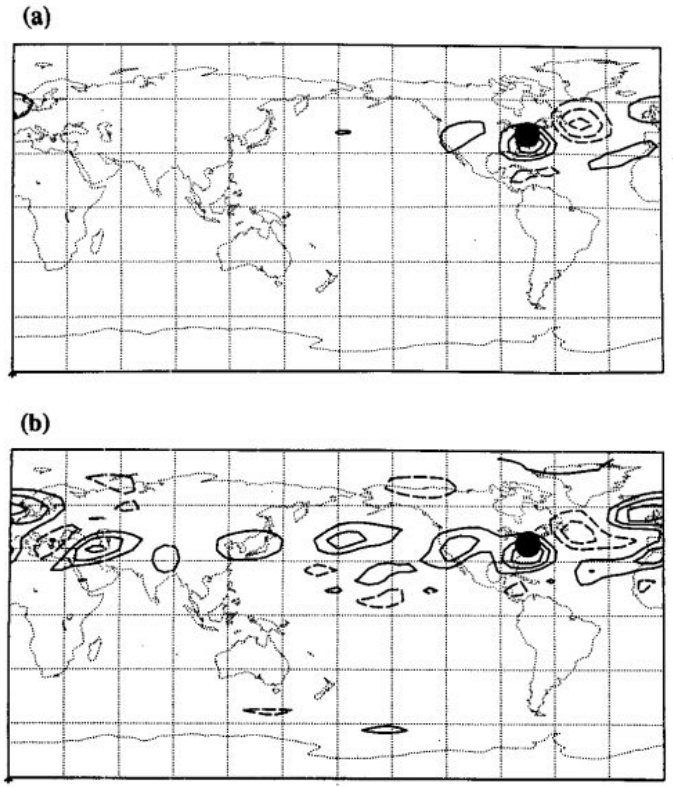

FIG. 15. The model vorticity anomaly for the forcing centered at (40°N, 75°W) at (a) day 4 and (b) day 12. Contour conventions as in Fig. 12.

e) Jato norte africano - asiático

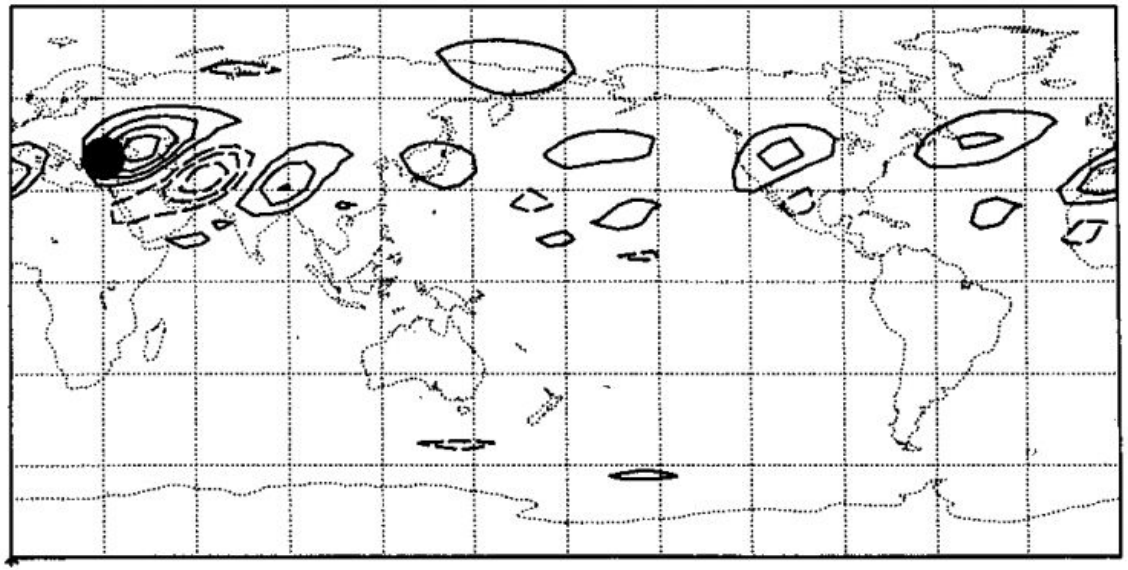

FIG. 16. The model vorticity anomaly at day 12 for the forcing at (40°N, 30°E). Contour conventions as in Fig. 12.

6. Conclusões

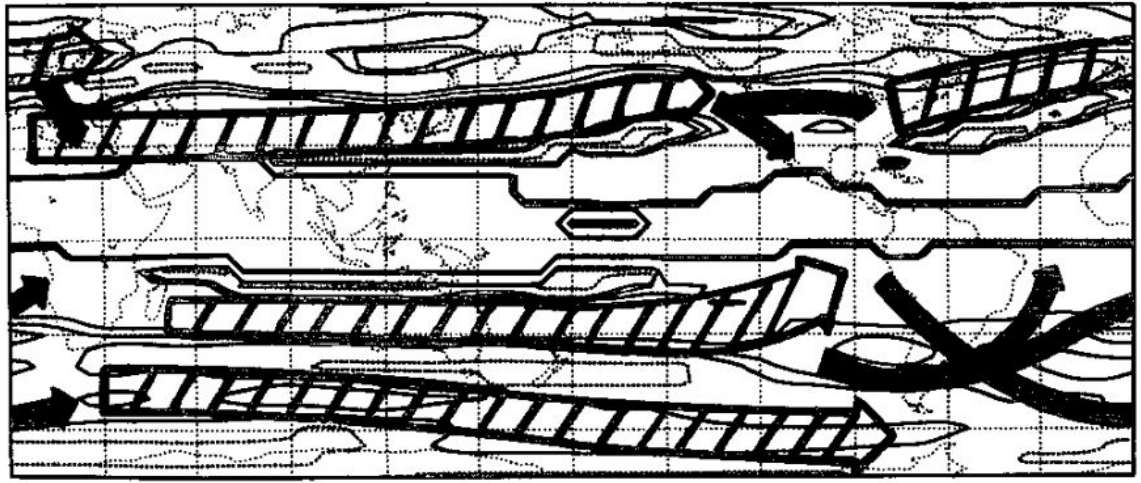

FIG. 17. A schematic summary of the waveguides, shown by the cross-hatched shafted arrows, and the preferred propagation patterns, indicated by the single-shafted arrows, deduced from the range of experiments. The background contours are those for K_s equal to 0, 4, 5, 6, and 25–30 taken from Fig. 11c.

7. Referências

REFERENCES

Berbery, E. H., J. Nogués-Paegle, and J. D. Horel, 1992: Wavelike Southern Hemisphere extratropical teleconnections. *J. Atmos. Sci.*, **49,** 155–177.

Blackmon, M. L., 1976: A climatological spectral study of the geopotential height of the Northern Hemisphere. *J. Atmos. Sci.*, **33,** 1607–1623.

——, Y.-H. Lee, and J. M. Wallace, 1984a: Horizontal structure of 500 mb height fluctuations with long, intermediate and short time scales. *J. Atmos. Sci.*, **41,** 961–979.

——, ——, ——, and H.-H. Hsu, 1984b: Time variation of 500 mb height fluctuations with long, intermediate and short time scales as deduced from lag-correlation statistics. *J. Atmos. Sci.*, **41,** 981–991.

Farrara, J. D., M. Ghil, and C. R. Mechoso, 1989: Empirical orthogonal functions and multiple flow regimes in the Southern Hemisphere winter. *J. Atmos. Sci.*, **46,** 3219–3223.

Gao, X. H., and J. L. Stanford, 1988: Possible feedback path for low-frequency atmospheric oscillations. *J. Atmos. Sci.*, **45,** 1425–1432.

Held, I. M., R. L. Panetta, and R. T. Pierrehumbert, 1985: Stationary external Rossby waves in vertical shear. *J. Atmos. Sci.*, **42,** 865–883.

Hoskins, B. J., and D. J. Karoly, 1981: The steady linear response of a spherical atmosphere to thermal and orographic forcing. *J. Atmos. Sci.*, **38,** 1179–1196.

——, and T. Ambrizzi, 1993: Rossby wave propagation on a realistic longitudinally varying flow. *J. Atmos. Sci.*, **50,** 1661–1671.

Hsu, H.-H., and S.-H. Lin, 1992: Global teleconnections in the 250-mb streamfunction field during the Northern Hemisphere winter. *Mon. Wea. Rev.*, **120,** 1169–1190.

Kidson, J. W., 1988: Interannual variations in the Southern Hemisphere circulation. *J. Climate,* **1,** 1177–1198.

——, 1991: Intraseasonal variations in the Southern Hemisphere circulation. *J. Climate,* **4,** 939–953.

Kousky, V. E., and G. D. Bell, 1992: Atlas of Southern Hemisphere 500-mb Teleconnection Patterns Derived from National Meteorological Center Analyses. NOAA Atlas 9, U.S. Department of Commerce, 90 pp.

Lau, K.-M., and L. Peng, 1992: Dynamics of atmospheric teleconnections during the northern summer. *J. Climate,* **5,** 140–158.

Mo, K. C., and G. H. White, 1985: Teleconnections in the Southern Hemisphere. *Mon. Wea. Rev.*, **113,** 22–37.

——, and M. Ghil, 1987: Statistics and dynamics of persistent anomalies. *J. Atmos. Sci.*, **44,** 877–901.

Schubert, S. D., 1986: The structure, energetics and evolution of the dominant frequency-dependent three-dimensional atmospheric modes. *J. Atmos. Sci.*, **43,** 1210–1237.

Trenberth, K. E., 1979: Interannual variability of the 500 mb zonal mean flow in the Southern Hemisphere. *Mon. Wea. Rev.*, **107,** 1515–1527.

——, 1980: Planetary waves at 500 mb in the Southern Hemisphere. *Mon. Wea. Rev.*, **108,** 1378–1389.

——, 1981a: Interannual variability of the Southern Hemisphere 500 mb flow: Regional characteristics. *Mon. Wea. Rev.*, **109,** 127–136.

——, 1981b: Observed Southern Hemisphere eddy statistics at 500 mb frequency and spatial dependence. *J. Atmos. Sci.*, **38,** 2585–2605.

——, 1986: An assessment of the impact of transient eddies on the zonal flow during a blocking episode using localized Eliassen-Palm flux diagnostics. *J. Atmos. Sci.*, **43,** 2070–2087.

——, 1991: Storm tracks in the Southern Hemisphere. *J. Atmos. Sci.*, **48,** 2159–2178.

Wallace, J. M., and D. S. Gutzler, 1981: Teleconnections in the geopotential height field during the Northern Hemisphere winter. *Mon. Wea. Rev.*, **109,** 785–812.

——, and M. L. Blackmon, 1983: Observations of low-frequency atmospheric variability. *Large-Scale Dynamical Processes in the Atmosphere.* B. J. Hoskins and R. P. Pearce, Eds., Academic Press, 55–94.

——, G.-H. Lim, and M. L. Blackmon, 1988: On the relationship between cyclone tracks, anticyclone tracks and baroclinic waveguides. *J. Atmos. Sci.*, **45,** 439–462.

Webster, P. J., and J. R. Holton, 1982: Cross-equatorial response to middle latitude forcing in zonally varying basic state. *J. Atmos. Sci.*, **39,** 722–733.